

# Quantum Krylov Subspace Diagonalization via Time Reversal Symmetries

Nicola Mariella,<sup>1,\*</sup> Enrique Rico,<sup>2,3,4,5</sup> Adam Byrne,<sup>1,6</sup> and Sergiy Zhuk<sup>1</sup>

<sup>1</sup>IBM Quantum, IBM Research Europe - Dublin

<sup>2</sup>EHU Quantum Center and Department of Physical Chemistry,  
University of the Basque Country UPV/EHU, P.O. Box 644, 48080 Bilbao, Spain

<sup>3</sup>DIPC - Donostia International Physics Center,

Paseo Manuel de Lardizabal 4, 20018 San Sebastián, Spain

<sup>4</sup>IKERBASQUE, Basque Foundation for Science, Plaza Euskadi 5, 48009 Bilbao, Spain

<sup>5</sup>European Organization for Nuclear Research (CERN),

Theoretical Physics Department, CH-1211 Geneva, Switzerland

<sup>6</sup>School of Mathematics, Trinity College Dublin, Ireland

Krylov quantum diagonalization methods have emerged as a promising use case for quantum computers. However, many existing implementations rely on controlled operations, which pose challenges to near-term quantum hardware. We introduce a novel protocol, which we call *Krylov Time Reversal* (KTR), which avoids these bottlenecks by exploiting the time-reversal symmetry in Hamiltonian evolution. Using symmetric time dynamics, we show that it is possible to recover real-valued Krylov matrix elements, which significantly reduces the circuit depth and enhances compatibility with shallow quantum architectures. We validate our method through numerical simulations on paradigmatic Hamiltonians exhibiting time-reversal symmetry, including the transverse-field Ising model and a lattice gauge theory, demonstrating accurate spectral estimation and favorable circuit constructions.

## I. INTRODUCTION

As quantum devices transition steadily into the pre-fault-tolerant era, there is growing interest in algorithms that can leverage limited coherence times and circuit depths while still extracting useful spectral information from quantum systems. Among the most promising techniques for the estimation of ground state energy in near-term devices are *quantum subspace diagonalization* methods [1–15]. These techniques aim to construct low-dimensional subspaces whose diagonalization yields accurate approximations of the extremal eigenvalues of the full-system Hamiltonian. The most suitable choice of subspace for near-term quantum computers is that generated by powers of the real-time evolution operator, which can be efficiently approximated on existing quantum devices. Methods using this subspace are often referred to as *Krylov Quantum Diagonalization* (KQD) methods [1–7], and possess rigorous convergence guarantees, even in the presence of noise [16, 17].

In many KQD protocols, the construction of Krylov overlap matrices requires controlled unitary operations, which are challenging to implement on near-term quantum devices [18]. Recent efforts have focused on developing control-free or control-light versions of KQD that are better suited to the constraints of current quantum hardware. In particular, schemes inspired by the theory of holomorphic functions have demonstrated how spectral properties can be extracted using phase-sensitive measurements with locally controlled operations [19]. For

Hamiltonians with global  $U(1)$  or global  $SU(2)$  symmetries, multifidelity protocols can be used to avoid controlled unitary operations [5], and have been experimentally demonstrated on 56 qubits [11]. Other sampling-based KQD methods, which require assumptions on the sparsity of the ground state, use only real-time evolutions and sampling in the computational basis, and have been performed experimentally on 85 qubits [12]. Work in super-Krylov methods [20] has also shown how advanced basis construction techniques, tailored to the structure of quantum Hamiltonians, can enhance the precision of subspace approximations while reducing the circuit depth.

Motivated by these developments, we propose a novel KQD algorithm for Hamiltonians with time-reversal symmetry in this letter, which avoids the need for controlled unitary operations. Specifically, the time-symmetric evolution can be exploited to recover real-valued overlap information between the Krylov states. Thus, the method, which we call *Krylov Time Reversal* (KTR), is desirable for implementation in shallow and noisy devices while preserving the favorable convergence properties of KQD. The proposed algorithm builds on the insights of low-control measurement approaches [21] and compilation techniques [22], as well as the theoretical structure of KQD [1–7] and its recent advances [20]. Our contribution is a hybrid algorithmic framework that is both resource-efficient and theoretically grounded, offering a path forward for quantum spectral estimation in the near term.

The paper is organized as follows: [Section II](#) outlines the foundational principles of KQD; [Section III](#) presents our proposal; [Section IV](#) describes the construction of initial states; and [Section V](#) evaluates the approach by benchmarking on two representative models.

---

\* nicola.mariella@ibm.com

## II. KRYLOV QUANTUM DIAGONALIZATION

KQD is a variational framework that approximates the low-lying eigenstates of a given Hamiltonian by constructing a *Krylov subspace* [23, 24] generated by the time evolution applied to some reference state. We introduce the key aspects of KQD that are relevant to our work.

Consider an arbitrary many-body Hamiltonian  $\mathcal{H}(\gamma)$  depending on the parameter  $\gamma \in \mathbb{R}$ . Let  $|v_0\rangle$  be a fixed initial state. We define the time evolution (in practice, Trotterized) by

$$|v(t)\rangle := \exp(-it\mathcal{H})|v_0\rangle, \quad (1)$$

for  $t \in \mathbb{R}$ , so that  $|v(0)\rangle = |v_0\rangle$ . Let  $t_a, t_b \in \mathbb{R}$  be the time displacements. We note the following properties:

$$\langle v(t_a)|v(t_b)\rangle = \langle v_0|\exp(-i(t_b - t_a)\mathcal{H})|v_0\rangle \quad (2a)$$

$$= \langle v_0|v(t_b - t_a)\rangle, \quad (2b)$$

$$\langle v(t_a)|\mathcal{H}|v(t_b)\rangle = \langle v_0|\exp(it_a\mathcal{H})\mathcal{H}|v(t_b)\rangle \quad (2c)$$

$$= \langle v_0|\mathcal{H}|v(t_b - t_a)\rangle. \quad (2d)$$

The identity in (2c) also holds for any operator  $K$  that commutes with the Hamiltonian, that is,  $\langle v(t_a)|K|v(t_b)\rangle = \langle v_0|K|v(t_b - t_a)\rangle$ .

Let  $\mathcal{I} \subset \mathbb{R}$  be a finite set of time displacements of finite cardinality  $m$  such that  $(t_a, t_b) \in \mathcal{I} \times \mathcal{I}$ . The overlaps in (2a) and (2c) can be used to construct the  $m \times m$  matrices<sup>1</sup>  $A, B$ , whose entries are given by

$$A_{a,b} = \langle v(t_a)|\mathcal{H}|v(t_b)\rangle, \quad (3a)$$

$$B_{a,b} = \langle v(t_a)|v(t_b)\rangle, \quad (3b)$$

where natural ordering is assumed for the time displacements. It follows that both matrices  $A$  and  $B$  are *Hermitian-Toeplitz*<sup>2</sup> [25]. The canonical method is then concluded by solving the *generalized eigenvalue problem* [24]  $A\mathbf{x} = \lambda B\mathbf{x}$ , to obtain the low-lying spectrum of  $\mathcal{H}$ .

The entries for the matrices in (3a) and (3b) are, in general, in the complex field  $\mathbb{C}$ , so their estimation requires the *Hadamard test* [26, 27]. However, its practical implementation encounters difficulties mainly due to the need for high-fidelity controlled operations, which render this approach unreliable on *Noise-Intermediate-Scale Quantum* (NISQ) devices. In this work, we show that, under certain assumptions on the Hamiltonian  $\mathcal{H}(\gamma)$ , these overlaps are real-valued and can be obtained as quantum expectations.

## III. FORMULATION

We consider the set of Hamiltonians for which there exists a *Hermitian involutory* operator  $T$  such that

$$T\mathcal{H}(\gamma) = -\mathcal{H}(\gamma)T, \quad (4)$$

for all  $\gamma \in \mathbb{R}$ . That is, we require the anticommutator relation  $\{T, \mathcal{H}\} = 0$ , independently of the parameter  $\gamma \in \mathbb{R}$ . In linear algebra, this condition is known as *generalized skew-centrosymmetry* [28]. We observe the following property of the time evolution,

$$Te^{-it\mathcal{H}}T = e^{-itT\mathcal{H}T} = e^{it\mathcal{H}}. \quad (5)$$

That is, the conjugate action of  $T$  has the effect of *reversing the time evolution*, so we call the operator  $T$  the *time reversal operator*<sup>3</sup>. Given a Hamiltonian, if the operator  $T$  exists, then it is not necessarily unique<sup>4</sup>. However, for the main part of this work, we consider a single (arbitrary) choice of such an operator.

The initial state  $|v_0\rangle$  for the time evolution in (1), is assumed to be stabilized by the action of  $T$  up to a constant sign flip<sup>5</sup>, that is

$$T|v_0\rangle = c|v_0\rangle, \quad (6)$$

with  $c \in \{\pm 1\}$ . Moreover, it can be shown that  $|v_0\rangle$  consists of a linear combination of eigenvectors of  $T$  from the same eigenspace<sup>6</sup>. The formal construction of the initial state is treated in Section IV.

The first key result (proof in Section A) reveals a convenient formulation for the inner product in (2a).

**Lemma III.1.** *Consider the Hamiltonian  $\mathcal{H}$  and a Hermitian involutory anticommuting operator  $T$  fulfilling (6). Let  $t_a, t_b \in \mathbb{R}$  and let  $h = \frac{t_b - t_a}{2}$ , then*

$$\langle v(t_a)|v(t_b)\rangle = c \langle v(h)|T|v(h)\rangle \in \mathbb{R}, \quad (7)$$

with  $c = \langle v_0|T|v_0\rangle \in \{\pm 1\}$ .

We observe that the LHS of the expression in (7) corresponds to the entry  $B_{a,b}$  of the Gram matrix in (3b). Put differently, this construction yields entries that are guaranteed to be real, which can be obtained without requiring a controlled time evolution. The RHS of (7) is an expectation with the Hermitian observable  $T$ . As an additional benefit, we observe that the time evolution from  $t_b - t_a$  in (2a) to  $h = (t_b - t_a)/2$  in (7) has halved.

We turn to the second key result (proof in Section A).

<sup>1</sup> It is assumed that the dimension  $m$  (i.e., the number of Krylov vectors) depends polynomially on the number of qubits. Thus, any further computation on such objects is classical.

<sup>2</sup> An  $n \times n$  Toeplitz matrix  $A$  is defined by the entries  $A_{i,j} = a_{i-j}$  depending on the difference  $i - j$ . If, in addition,  $A$  is Hermitian, then a selected row or column defines  $A$ .

<sup>3</sup> This should not be confused with the time reversal in physics, which is obtained from the action of an anti-unitary operator.

<sup>4</sup> We expand on the subject in Section B.

<sup>5</sup> The constant  $c \in \{\pm 1\}$  is unphysical when interpreted as a global phase; however, it will become relevant in Section IV.

<sup>6</sup> Since  $T$  is Hermitian-involutory and  $\{\mathcal{H}, T\} = 0$  with  $\mathcal{H} \neq 0$ , then its eigenvalues are  $\{\pm 1\}$ , so we have two eigenspaces.

**Lemma III.2.** *Assuming the same conditions of Lemma III.1, let  $K$  be a Hermitian operator such that  $[K, \mathcal{H}] = 0$  and  $\{K, T\} = 0$ . Then*

$$\langle v(t_a) | K | v(t_b) \rangle = ic \langle v(h) | (iKT) | v(h) \rangle \in i\mathbb{R}, \quad (8)$$

with  $c = \langle v_0 | T | v_0 \rangle \in \{\pm 1\}$ .

As a corollary of Lemma III.2, when  $K = \mathcal{H}$  we obtain the entries of the matrix  $A$  defined in (3a), that is,

$$A_{a,b} = ic \langle v(h) | (i\mathcal{H}T) | v(h) \rangle \in i\mathbb{R}. \quad (9)$$

Similarly to the result in Lemma III.1, we obtain the entries of the matrix  $A$  (defined in (3a)) as expectations of the Hermitian observable  $i\mathcal{H}T$ . The benefit of halved time evolution persists and could also be favorable for *tensor networks* (TN) [29].

The matrices  $A$  and  $B$  are Hermitian-Toeplitz, which is reflected by the fact that the state  $|v(h)\rangle$  (which appears in the RHS of (7) and (8)) depends solely on the difference  $t_b - t_a$ . Such structures can be defined by their first row<sup>7</sup>, so we need to evaluate a linear number of expectations in the number of Krylov vectors.

To conclude, we examine the spectral characterization of the Hamiltonians concerning this work. Given the eigenvalue equation  $\mathcal{H}|\psi_i\rangle = \lambda_i|\psi_i\rangle$ , we observe that  $\mathcal{H}(T|\psi_i\rangle) = -\lambda_i(T|\psi_i\rangle)$ , so  $\langle\psi_i|(T|\psi_i\rangle) = 0$  when  $\lambda_i \neq 0$ . That is, the spectrum is mirrored, so the ground and the most excited energies have the same magnitude.

#### IV. INITIAL STATE $|v_0\rangle$

We study the general construction for the initial state  $|v_0\rangle$ , fulfilling (6). In addition, we obtain another initial state  $|v_0^\perp\rangle$ , orthogonal to the former, that satisfies the same property. Let  $T$  be a time reversal operator for the Hamiltonian  $\mathcal{H}$  and define

$$P := \frac{T + \mathbb{I}}{2}, \quad P^\perp := \mathbb{I} - P = \frac{\mathbb{I} - T}{2}, \quad (10)$$

as the (complementary<sup>8</sup>) *orthogonal projections* [25] induced by  $T$ . As a result of the direct sum decomposition  $V \oplus V^\perp$  of the underlying vector space, any state  $|\varphi\rangle$  can be expressed as  $|\varphi\rangle = P|\varphi\rangle + P^\perp|\varphi\rangle$ . Then, for any state  $|\varphi\rangle$  such that  $\langle\varphi|P|\varphi\rangle \neq 0$ , we have  $T|v_0\rangle = |v_0\rangle$ , with  $|v_0\rangle := \xi P|\varphi\rangle$  and  $1/\xi^2 = \langle\varphi|P|\varphi\rangle$ ,  $\xi > 0$ . In addition, if  $\langle\varphi|P^\perp|\varphi\rangle \neq 0$ , then  $T|v_0^\perp\rangle = -|v_0^\perp\rangle$ , with  $|v_0^\perp\rangle := \frac{\xi}{\sqrt{\xi^2 - 1}} P^\perp|\varphi\rangle$ . In addition, we have the orthogonality  $\langle v_0 | v_0^\perp \rangle = 0$ , when  $|v_0\rangle$  and  $|v_0^\perp\rangle$  are defined. This shows that the constant  $c \in \{\pm 1\}$ , concerning

Lemma III.1 and Lemma III.2, depends on which projector in (10) is used for the preparation of the initial state.

In summary, one can apply either the projector  $P$  or its complement  $P^\perp$  on some state  $|\varphi\rangle$  to obtain, upon normalization (assuming a non-zero projection), the initial state  $|v_0\rangle$  that fulfills (6).

We analyze a practical setup. Consider the operator  $T$  and a state  $|\varphi\rangle$  that can be efficiently represented as a *matrix product operator* (MPO) [30] and a *Matrix Product State* (MPS) [29] respectively. Then, after classically obtaining the projections  $P|\varphi\rangle$  and  $P^\perp|\varphi\rangle$  as MPS states, the corresponding circuits can be prepared using a compiler technique [31, 32]. More generally, the same concept can be extended to initial states represented by TN. A practical circuit construction for projection operators is discussed in Section D. In Section C, we reveal an indirect connection with the Hadamard test.

## V. EXPERIMENTS

We assess the validity of the method via TN simulations<sup>9</sup>, generating Krylov vectors through MPS time evolutions [35]. We employ as references the canonical KQD<sup>10</sup> and the *density matrix renormalization group* (DMRG) [36], observing strong agreement; all further details on the setting up of the quantum Krylov subspace diagonalization (e.g., time step choice, spectral thresholding) are addressed in the existing literature [1, 16]. We proceed with the two models that follow.

### A. Case: The transverse-field Ising model

We construct an initial state  $|v_0\rangle$  for the *Transverse-Field Ising Model* (TFIM), which is guaranteed to have sufficient overlap with the relevant eigenspaces, while reducing the cost of circuit implementation. Recall the definition of the Hamiltonian

$$\mathcal{H}(\gamma) = - \sum_i \sigma_i^x \sigma_{i+1}^x - \gamma \sum_i \sigma_i^z, \quad (11)$$

which, for simplicity, is assumed on the Hilbert space of  $n = 4d$  qubits for some positive integer  $d$ . The two terms in (11), are denoted as the base terms  $\mathcal{H}_0$  and the driving terms  $\mathcal{H}_d$ , respectively, so  $\mathcal{H} = \mathcal{H}_0 + \gamma\mathcal{H}_d$ . For the involutory operator  $T = (\sigma^y \otimes \sigma^x)^{\otimes(2d)}$ , it can be verified that  $\{T, \mathcal{H}(\gamma)\} = 0$  for all  $\gamma \in \mathbb{R}$ .

<sup>7</sup> In practice, assuming  $t_1 = 0$ , the first row of  $B$  is obtained from the expectations  $B_{1,j} = \langle v(h_j) | T | v(h_j) \rangle$  with  $h_j = \frac{t_j - t_1}{2} = \frac{t_j}{2}$  and  $t_j \in \mathbb{Z}$ . Then,  $B_{i+1,j+1} = B_{1,|i-j|}$  for  $i > 1$ .

<sup>8</sup> That is  $P^\perp = \mathbb{I} - P$  with  $P^2 = \mathbb{I}$  and  $P^\dagger = P$ , so  $PP^\perp = 0$ .

<sup>9</sup> The implementation is based on the library *iTensor* [33]. Time evolutions are approximated using the second-order Trotterization [34], and MPSs have a maximum bond dimension of 500.

<sup>10</sup> We note that in the case of KQD, the overlap matrices typically have complex entries, so, its quantum circuit implementation requires the Hadamard test.

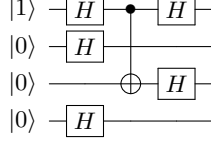


**FIG. 1:** Block circuit (case  $r = 4$  qubits) for the preparation of the state  $-|w_0\rangle$  in (12). The product  $|v_0\rangle = |w_0\rangle^{\otimes s}$  yields the initial states.

Assume that the parameter  $|\gamma|$  is small enough for the term  $\mathcal{H}_0$  to dominate. Let the state  $|w_0\rangle$ , on  $r = n/s = 4d/s$  qubits with  $s$  a positive divisor of  $d$ , be defined by

$$|w_0\rangle = \frac{1}{\sqrt{2}} \left( (-1)^{r/4} |+\rangle^{\otimes r} + |-\rangle^{\otimes r/2} \right). \quad (12)$$

Hence, we obtain an initial state  $|v_0\rangle = |w_0\rangle^{\otimes s}$  fulfilling (6), as the  $s$ -fold product of blocks. We justify this construction for its overlap with the ground state (possibly degenerate) of the base term  $\mathcal{H}_0$ , which is dominant for small  $|\gamma|$ . In fact, we can verify that  $|\langle +|^{\otimes n} |v_0\rangle| = 1/\sqrt{2^s}$ . So, for relatively small divisors  $s$  of the positive integer  $d$ , we guarantee the required symmetry and overlap with the ground state. Another rationale is to avoid generating long-range entanglement throughout the system, although methods based on dynamic circuits are available [37]. A formal treatment of this kind of structure is presented in Section D. The experimental results for this construction are reported in Figure 2.

The expression for the observable  $i\mathcal{H}T$ , determining the expectation in (9), follows directly from the identity  $i\sigma^x\sigma^y\sigma^z = -\mathbb{I}$ , that is,

$$i\mathcal{H}T = \sum_i (\sigma_i^z \sigma_i^y) \sigma_{i+1}^x T + \gamma \sum_i (\sigma_i^y \sigma_i^x) T. \quad (13)$$

### B. Case: $\mathbb{Z}_2$ gauge Higgs model

We benchmark a model from high-energy physics: a *lattice gauge theory* (LGT) Hamiltonian, specifically the  $\mathbb{Z}_2$  gauge Higgs model [38–40]. Such models capture essential features of gauge-invariant dynamics on a discretized space, providing a rich testbed for exploring quantum many-body phenomena. Denoting, respectively,  $\mathcal{V}$  and  $\mathcal{L}$ , the sets of vertices and links of the lattice, the Hamiltonian is defined by

$$\mathcal{H}(\mu, g) = - \sum_{i \in \mathcal{L}} \sigma_{i-1}^z \sigma_i^z \sigma_{i+1}^z - \mu \sum_{j \in \mathcal{V}} \sigma_j^x - g \sum_{k \in \mathcal{L}} \sigma_k^x, \quad (14)$$

where the interaction term corresponds to the minimal coupling of vertices (matter) qubits and links (gauge) qubits; the onsite term on the vertices characterizes the

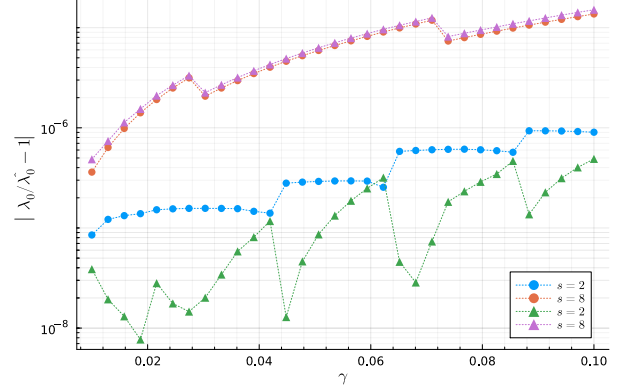


**FIG. 2:** Relative error of the ground energy  $\lambda_0$  for the TFIM on  $n = 64$  qubits with  $m = 128$  (MPS) Krylov vectors and  $s$  the number of blocks  $|w_0\rangle$ . References for  $\hat{\lambda}_0$  are KQD ( $\bullet$ ) and DMRG ( $\blacktriangle$ ), with initial state  $|\varphi\rangle = |+\rangle^{\otimes n}$ .

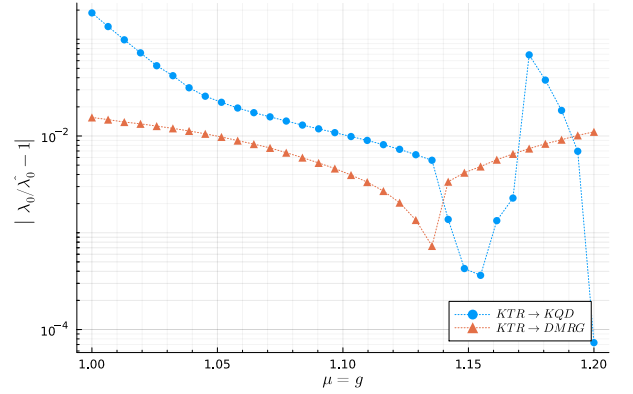


**FIG. 3:** Relative error for the  $\mathbb{Z}_2$  gauge Higgs model on  $n = 64$  qubits, relative to the ground energy for the sector  $G|\psi\rangle = |\psi\rangle$ . We considered  $m = 80$  Krylov vectors (MPS) and  $s = 2$  blocks  $|w_0\rangle$ .

energy cost to excite a matter qubit, while the onsite term on the links describes the energy cost to excite a gauge qubit. A time reversal operator is  $T = (\sigma^y)^{\otimes n}$ . The gauge symmetries are generated by the operators  $G_k$  [38] and let  $G$  be their averaged sum, which can be verified to anticommute with  $T$ . In relation to Section IV, we start with the state  $|\varphi\rangle = |+\rangle^{\otimes n}$ , which is gauge invariant since  $G|\varphi\rangle = |\varphi\rangle$ . We aim at obtaining the ground energy for the sector (invariant subspace) determined by the latter. The initial state is  $|v_0\rangle = \xi P |\varphi\rangle = \xi(|\varphi\rangle + T|\varphi\rangle)/2$ , but  $G(T|\varphi\rangle) = -T|\varphi\rangle$ , so  $|v_0\rangle$  is a superposition from two sectors. However, if  $\langle \varphi | \mathcal{H} | \varphi \rangle < 0$ , then  $(\langle \varphi | T) \mathcal{H} (T | \varphi \rangle) = -\langle \varphi | \mathcal{H} | \varphi \rangle > 0$ , so the former sector is favored by the Krylov method. This is the case since  $\langle \varphi | \mathcal{H} | \varphi \rangle = \langle + |^{\otimes n} \mathcal{H} | + \rangle^{\otimes n} < 0$  for positive parameters  $\mu, g$ . Finally, as in Section V A, we break down the initial state  $|v_0\rangle$  into an  $s$ -fold product of blocks  $|w_0\rangle$ . The experimental results for this construction are reported in Figure 3.

## ACKNOWLEDGMENTS

The data generated from quantum simulations and supporting this study are available from the authors upon reasonable request.

N.M. is grateful to Antonio Mezzacapo (IBM Research) and Pawel Wocjan (IBM Research) for useful technical discussions.

E.R. acknowledges the financial support received from the IKUR Strategy under the collaboration agreement between the Ikerbasque Foundation and UPV/EHU on behalf of the Department of Education of the Basque Government. E.R. acknowledges support from the BasQ strategy of the Department of Science, Universities, and Innovation of the Basque Government. E.R. is supported by the grant PID2021-126273NB-I00 funded by MCIN/AEI/10.13039/501100011033 and by “ERDF A way of making Europe” and the Basque Government through Grant No. IT1470-22. This work was supported by the EU via QuantERA project T-NiSQ grant PCI2022-132984 funded by MCIN/AEI/10.13039/501100011033 and by the European Union “NextGenerationEU”/PRTR. This work has been financially supported by the Ministry of Economic Affairs and Digital Transformation of the Spanish Government through the QUANTUM ENIA project, called Quantum Spain project, and by the European Union through the Recovery, Transformation, and Resilience Plan – NextGenerationEU within the framework of the Digital Spain 2026 Agenda.

This work has been partially funded by the Eric & Wendy Schmidt Fund for Strategic Innovation through the CERN Next Generation Triggers project under grant agreement number SIF-2023-004.

## Appendix A: Proofs not included in the main text

We present the proofs of the main results. We recall that  $T$  is a Hermitian involutory operator such that  $\{\mathcal{H}, T\} = 0$ , and that the initial state  $|v_0\rangle$  fulfills the property of  $T|v_0\rangle = c|v_0\rangle$  with  $c \in \{\pm 1\}$ . For time displacements  $t_a, t_b \in \mathbb{R}$ , the half difference is  $h = (t_b - t_a)/2$ .

*Proof of Lemma III.1.*

$$\langle v(t_a)|v(t_b)\rangle \stackrel{(2a)}{=} \langle v_0|v(t_b - t_a)\rangle \quad (\text{A1a})$$

$$= \langle v_0|e^{-i h \mathcal{H}}|v(h)\rangle \quad (\text{A1b})$$

$$\stackrel{(5)}{=} \langle v_0|T e^{i h \mathcal{H}} T|v(h)\rangle \quad (\text{A1c})$$

$$\stackrel{(6)}{=} c \langle v_0|e^{i h \mathcal{H}} T|v(h)\rangle \quad (\text{A1d})$$

$$= c \langle v(h)|T|v(h)\rangle. \quad (\text{A1e})$$

□

*Proof of Lemma III.2.* We proceed in such a way that the inner product becomes a quadratic form, so

$$\langle v(t_a)|K|v(t_b)\rangle \stackrel{(2c)}{=} \langle v_0|K|v(t_b - t_a)\rangle \quad (\text{A2a})$$

$$= \langle v_0|K e^{-i h \mathcal{H}}|v(h)\rangle \quad (\text{A2b})$$

$$\stackrel{(5)}{=} \langle v_0|K T e^{i h \mathcal{H}} T|v(h)\rangle \quad (\text{A2c})$$

$$= - \langle v_0|T K e^{i h \mathcal{H}} T|v(h)\rangle \quad (\text{A2d})$$

$$\stackrel{(6)}{=} -c \langle v_0|K e^{i h \mathcal{H}} T|v(h)\rangle \quad (\text{A2e})$$

$$= -c \langle v_0|e^{i h \mathcal{H}}(K T)|v(h)\rangle \quad (\text{A2f})$$

$$= i c \langle v(h)|i K T|v(h)\rangle. \quad (\text{A2g})$$

Finally, since the Hermitian operators  $K$  and  $T$  anti-commute, then  $(i K T)^\dagger = -i T K = i K T$ , hence  $i K T$  is Hermitian. □

## Appendix B: Time reversal symmetry

We provide a construction for Hamiltonians that fulfills the time-reversal symmetry. Let  $\mathcal{G}_n = \{\mathbb{I}, \sigma^x, \sigma^y, \sigma^z\}^{\otimes n}$  be the set of  $n$ -qubit Pauli strings. For the remainder of this section, we consider the class of Hamiltonians defined by a linear combination of Pauli strings, that is,

$$\mathcal{H} = \sum_i h_i \sigma_i, \quad (\text{B1})$$

with coefficients  $h_i \in \mathbb{R}$ . The result that follows is a generalization of the LGT case in Section V B.

**Lemma B.1.** *Let  $\{\sigma^a, \sigma^b, \sigma^c\}$  be the image of any bijection on the set of Paulis. Consider the case of the Hamiltonian in (B1), when each term consists of an odd number of Paulis from the set  $\{\sigma^a, \sigma^c\}$ <sup>11</sup>. Let  $T = \prod_{i=1}^n \sigma_i^b$  (so  $T = T^\dagger$  and  $T^2 = \mathbb{I}$ ), then we have  $T \mathcal{H} T = -\mathcal{H}$ .*

We remark that the preceding lemma can be extended further by considering a family of mutually anticommuting Hermitian matrices instead of the set of Paulis. The proof will naturally follow from the next result.

We outline a general method for obtaining involutory Hermitian anticommuting operators by adapting the procedure proposed in [41][Section VIII], intended to identify the generators of Hermitian operators that commute with the

<sup>11</sup> This means that each term can also include the (tensor) factors

$\{\sigma^b, \mathbb{I}\}$ , but without any parity requirements.



Hamiltonian. We parameterize each term  $\sigma_i$  of  $\mathcal{H}$  using a binary vector  $(f_x | f_z)^\top \in \{0, 1\}^{2n}$ , where the bits of each component  $f_x, f_z$  are set according to the Pauli string configuration. For example  $\sigma^x \otimes \sigma^y \otimes \sigma^z \otimes \mathbb{I} \mapsto (1 \ 1 \ 0 \ 0 | 0 \ 1 \ 1 \ 0)^\top$ . The parameterizations of all terms of  $\mathcal{H}$  (with  $h_i \neq 0$ ) are collected as the rows of the parity matrix,

$$F = (F_x | F_z). \quad (\text{B2})$$

We solve the linear system  $F\mathbf{t} = \mathbf{1}$  over the field  $\mathbb{F}_2$  for  $\mathbf{t} = (t_z | t_x)^\top$ , where  $\mathbf{1}$  is the column vector of ones. When solutions exist, the binary vector  $\mathbf{t}$  represents the anticommuting and involutory Hermitian operator  $T$  for the time reversal. We note that the components of  $\mathbf{t}$  (that is,  $t_z, t_x$ ), appear in reversed order w.r.t. the columns of matrix  $F$  (i.e.  $F_x, F_z$ ). This construction mimics the interaction of non-commuting Pauli operators, so the equation  $(f_x | f_z)^\top \cdot (t_z | t_x)^\top = 1$ , over  $\mathbb{F}_2$ , holds when the represented operators anti-commute.

The linear system stated earlier is an instance of the *XOR satisfiability problem* (XORSAT) – a special case of the *boolean satisfiability problem* (SAT) [42]. Unlike the general SAT problem, which is NP-complete, XORSAT admits a polynomial-time solution via Gaussian elimination.

We demonstrate the above method applied to the *cluster Hamiltonian* [43] on a spin-1/2 chain. Let  $L$  be the  $(n-1) \times n$  matrix defined by  $L_{i,j} = \delta_{0 \leq (j-i) \leq 1}$ , and denote by  $\mathbb{I}_n$  the  $n \times n$  identity matrix. From the definition of the Hamiltonian

$$\mathcal{H} = -g_x \sum_{i=1}^n \sigma_i^x - g_{zz} \sum_i \sigma_i^z \sigma_{i+1}^z + g_{zxz} \sum_i \sigma_i^z \sigma_{i+1}^x \sigma_{i+2}^z, \quad (\text{B3})$$

we construct the  $(3n-3) \times (2n+1)$  augmented matrix for linear system  $F\mathbf{t} = \mathbf{1}$ , that is,

$$(F_x | F_z | \mathbf{1}) = \left( \begin{array}{c|c|c} \mathbb{I}_n & 0 & \mathbf{1} \\ 0 & L & \mathbf{1} \\ G_x & G_z & \mathbf{1} \end{array} \right), \quad (\text{B4})$$

where  $(G_x | G_z)$  describes the  $n-2$  terms of the form  $\sigma_i^z \sigma_{i+1}^x \sigma_{i+2}^z$ . However, it can be shown that the last block row is a linear combination (on  $\mathbb{F}_2$ ) of the first two blocks, so the system is taken to the *reduced row echelon form* (RREF) from this intermediate step,

$$\left( \begin{array}{c} \mathbb{I}_n \\ R \end{array} \right) \left( \begin{array}{c|c|c} \mathbb{I}_n & 0 & \mathbf{1} \\ 0 & L & \mathbf{1} \end{array} \right) = \left( \begin{array}{c|c|c} \mathbb{I}_n & 0 & \mathbf{0} \\ 0 & \mathbb{I}_{n-1} & \mathbf{1} \end{array} \right) (R\mathbf{1}), \quad (\text{B5})$$

where  $R$  is the  $(n-1) \times (n-1)$  upper-triangular matrix of ones (representing elementary row operations). It is noteworthy that the parity matrix in (B5) coincides with that of the TFIM, implying that the two Hamiltonians share the same anti-commutators. The vector  $R\mathbf{1}$  of row sums of the matrix  $R$  consists of alternating zeros and ones, that is  $(R\mathbf{1})_i = (1 - (-1)^{n-i})/2$ , for  $i = 1, 2, \dots, n-1$ . Now, note that the  $(2n-1)$ -th row vector (i.e., last) of the RHS matrix in (B5) is always of the form  $(0 \ 0 \dots 0 \ 1 \ 1 | 1)$ . Then, assuming  $n$  is even, by backward substitution, we obtain the solutions  $T_1 = (\sigma^y \otimes \sigma^z)^{\otimes \frac{n}{2}}$  and  $T_2 = (\sigma^z \otimes \sigma^y)^{\otimes \frac{n}{2}}$ .

As a negative example, we show that for the general *quantum Heisenberg model* given by the Hamiltonian<sup>13</sup>

$$\mathcal{H} = -\frac{1}{2} \sum_{j=1}^{n-1} (J_x \sigma_j^x \sigma_{j+1}^x + J_y \sigma_j^y \sigma_{j+1}^y + J_z \sigma_j^z \sigma_{j+1}^z), \quad (\text{B6})$$

the system  $F\mathbf{t} = \mathbf{1}$  has no solutions. Here, the symbols  $J_x, J_y, J_z \in \mathbb{R}$  denote the (arbitrary) coupling constants. The  $3(n-1) \times (2n+1)$  augmented matrix for the linear system is

$$(F_x | F_z | \mathbf{1}) = \left( \begin{array}{c|c|c} L & 0 & \mathbf{1} \\ 0 & L & \mathbf{1} \\ L & L & \mathbf{1} \end{array} \right). \quad (\text{B7})$$

In the attempt to obtain the RREF, by adding over  $\mathbb{F}_2$  the first two blocks of rows to the third one, we get the block row  $(0 | 0 | \mathbf{1})$ , which is inconsistent, so this Hamiltonian does not admit any anticommuting Hermitian operators.

<sup>12</sup> Here  $\mathbf{f} \cdot \mathbf{t}$  denotes the inner product of  $\mathbf{f}, \mathbf{t}$  on  $\mathbb{F}_2$ .

<sup>13</sup> For simplicity, we omit the terms related to the external field.

### Appendix C: Implicit Hadamard test

We establish the **Hadamard test** as a linear combination of expectations. We note that this scheme can also benefit other quantum methods that require the Hadamard test. In addition, we show that the symmetry for the initial state  $|v_0\rangle$  stated in (6) can be implicitly relaxed. First, we remind the structure of the Hadamard test and its relation to our work. As considered in Section IV, let  $|\varphi\rangle$  be an arbitrary initial state (i.e., not necessarily fulfilling (6)) and let  $U = \exp(-i(t_b - t_a)\mathcal{H})$  be the unitary corresponding to the time evolution for the time displacement  $t_b - t_a$ . The Hadamard test consists of the following circuit structure,

$$\begin{array}{c} |0\rangle \text{---} [H] \text{---} \bullet \text{---} [S^p] \text{---} [H] \text{---} \text{meter} \\ | \varphi \rangle \text{---} \text{---} [U] \text{---} \end{array} \quad (\text{C1})$$

which is used to estimate separately, the real and imaginary parts of  $\langle \varphi | U | \varphi \rangle$ , given by the identity

$$(1 - p) \Re \langle \varphi | U | \varphi \rangle + p \Im \langle \varphi | U | \varphi \rangle = \langle \sigma^z \rangle_p, \quad (\text{C2})$$

with  $p \in \{0, 1\}$ , and  $\langle \cdot \rangle_p$  the expectation of the given operator w.r.t. the state prepared by the circuit in (C1). We note that the quantity  $\langle \varphi | U | \varphi \rangle$  corresponds to the entry  $(a, b)$  of the Gram matrix in (3b), when the initial state  $|v_0\rangle$  is an arbitrary state (i.e., without the stabilizer property in (6)).

We introduce some notational details. For any square matrix  $A$  on  $\mathbb{C}$ , we define the Hermitian and skew-Hermitian parts respectively by

$$\text{Herm}(A) = \frac{A + A^\dagger}{2}, \quad \text{Skew}(A) = \frac{A - A^\dagger}{2}, \quad (\text{C3})$$

thus  $\text{Herm}(A) + \text{Skew}(A) = A$ . When the argument of  $\text{Herm}(\cdot), \text{Skew}(\cdot)$  is an operator time evolution, that is  $U = \exp(-it\mathcal{H})$ , then we have the special case

$$\text{Herm}(U) = \cosh(-it\mathcal{H}) = \cos(t\mathcal{H}), \quad (\text{C4a})$$

$$\text{Skew}(U) = \sinh(-it\mathcal{H}) = -i \sin(t\mathcal{H}), \quad (\text{C4b})$$

which is relevant for the theory that follows. Before proceeding further, we obtain some useful identities. These equations relate the Hamiltonian  $\mathcal{H}$  and its induced time evolution to the action of the projectors in (10).

**Lemma C.1.** *Consider the projectors in (10), induced by the time reversal operator  $T$ , then*

$$P\mathcal{H} = \mathcal{H}P^\perp, \quad P^\perp\mathcal{H} = \mathcal{H}P, \quad (\text{C5a})$$

$$P^\perp U P = \text{Skew}(U)P, \quad P U P^\perp = \text{Skew}(U)P^\perp, \quad (\text{C5b})$$

$$P U P = \text{Herm}(U)P, \quad P^\perp U P^\perp = \text{Herm}(U)P^\perp, \quad (\text{C5c})$$

$$P U P = P\sqrt{U}^\dagger T \sqrt{U} P, \quad P^\perp U P^\perp = -P^\perp \sqrt{U}^\dagger T \sqrt{U} P^\perp, \quad (\text{C5d})$$

with  $U = \exp(-it\mathcal{H})$  and  $\mathcal{H}$  the Hamiltonian.

*Proof.* The first set of equalities in (C5a) follows directly from the anticommutator relation  $\{\mathcal{H}, T\} = 0$ . We prove the leftmost in (C5b), then the other on the same line, and those in (C5c) follow similarly. So

$$P^\perp U P \stackrel{(10)}{=} \frac{1}{4} (U + UT - TU - TUT) \quad (\text{C6a})$$

$$\stackrel{(5)}{=} \frac{1}{2} \left( \frac{(U - U^\dagger)}{2} + \frac{(U - U^\dagger)}{2} T \right) \quad (\text{C6b})$$

$$= \text{Skew}(U)P. \quad (\text{C6c})$$

The identities in (C5d) can be deduced directly from the proof of Lemma III.1 and the definition of initial states in Section IV. Moreover, the  $\sqrt{U}$  corresponds to the half-time evolution with  $h = t/2$ , and the negative sign in the rightmost equality corresponds to the case  $c = -1$  in Lemma III.1.  $\square$



**Theorem C.1.** Let  $P, P^\perp$  be the projections defined in (10). Consider some state  $|\varphi\rangle$  assumed<sup>14</sup> not to be in the null space of the projections  $P, P^\perp$ . Let

$$|v(t)\rangle = \xi \exp(-it\mathcal{H}) P |\varphi\rangle, \quad (\text{C7a})$$

$$|v^\perp(t)\rangle = \frac{\xi}{\sqrt{\xi^2 - 1}} \exp(-it\mathcal{H}) P^\perp |\varphi\rangle, \quad (\text{C7b})$$

for some normalization coefficient  $\xi > 0$  (independent of time  $t$ ), such that  $\langle v(t)|v(t)\rangle = \langle v^\perp(t)|v^\perp(t)\rangle = 1$ . Then for any pair of time displacements  $t_a, t_b \in \mathbb{R}$ ,

$$\boxed{\frac{1}{\xi^2} \langle v(h)|T|v(h)\rangle - \left(1 - \frac{1}{\xi^2}\right) \langle v^\perp(h)|T|v^\perp(h)\rangle = \Re \langle \varphi|U|\varphi\rangle,} \quad (\text{C8})$$

with  $U = \exp(-i(t_b - t_a)\mathcal{H})$ ,  $h = (t_b - t_a)/2$ ,  $1/\xi^2 = \langle \varphi|P|\varphi\rangle$  and  $T$  the Hermitian-involutory operator defining the projection  $P$ .

As anticipated, the RHS of the claim in (C8) corresponds to the quantity estimated using the Hadamard test in (C2) with  $p = 0$  (i.e., the real part). The imaginary part can be estimated, up to a sign (i.e., possibly complex conjugate), using the identity

$$|\langle \varphi|U|\varphi\rangle|^2 = (\Re \langle \varphi|U|\varphi\rangle)^2 + (\Im \langle \varphi|U|\varphi\rangle)^2 \quad (\text{C9})$$

where the LHS is measured from the usual compute-uncompute circuit.

*Proof.* For a complex scalar  $z \in \mathbb{C}$  we denote by  $\Re z = (z + \bar{z})/2$  its real part. First, we note that

$$\Re \langle \varphi|U|\varphi\rangle = \langle \varphi|\text{Herm}(U)|\varphi\rangle. \quad (\text{C10})$$

So, we aim to prove the following

$$\frac{1}{\xi^2} \langle v(t_a)|v(t_b)\rangle - \left(1 - \frac{1}{\xi^2}\right) \langle v^\perp(t_a)|v^\perp(t_b)\rangle = \langle \varphi|\text{Herm}(U)|\varphi\rangle, \quad (\text{C11})$$

which, as a result of Lemma III.1, is equivalent to the claim in (C8).

By the complementarity of the projectors in (10), we have that  $P + P^\perp = \mathbb{I}$ , so by summing up the identities in (C5c) we obtain

$$PUP + P^\perp UP^\perp = \text{Herm}(U)(P + P^\perp) = \text{Herm}(U). \quad (\text{C12})$$

We recall that projectors  $P, P^\perp$  are used in the construction of the initial vectors  $|v_0\rangle, |v_0^\perp\rangle$  as outlined in Section IV. So, for example, we can rewrite the state in (C7a) as  $|v(t)\rangle = \exp(-it\mathcal{H})|v_0\rangle$ , with  $|v_0\rangle = \xi P|\varphi\rangle$ . Thus, from (C12), (C5d) and the definitions in (C7a) we obtain

$$\frac{1}{\xi^2} (\xi \langle \varphi|P)U(\xi P|\varphi\rangle) + \left(1 - \frac{1}{\xi^2}\right) (\xi^\perp \langle \varphi|P^\perp)U(\xi^\perp P^\perp|\varphi\rangle) = \frac{1}{\xi^2} \langle v_0|U|v_0\rangle + \left(1 - \frac{1}{\xi^2}\right) \langle v_0^\perp|U|v_0^\perp\rangle \quad (\text{C13a})$$

$$= \langle \varphi|\text{Herm}(U)|\varphi\rangle, \quad (\text{C13b})$$

with  $\xi^\perp = \frac{\xi}{\sqrt{\xi^2 - 1}}$ . The latter equation corresponds to (C11), which together with (C10) confirms the claim.  $\square$

We obtain the equivalent result to Theorem C.1 for the case of overlap with the Hamiltonian  $\mathcal{H}$ .

**Theorem C.2.** Under the same conditions and definitions as Theorem C.1, we have that

$$\boxed{\frac{i}{\xi^2} \langle v(h)|i\mathcal{H}T|v(h)\rangle - i \left(1 - \frac{1}{\xi^2}\right) \langle v^\perp(h)|i\mathcal{H}T|v^\perp(h)\rangle = i \Im \langle \varphi|U\mathcal{H}|\varphi\rangle.} \quad (\text{C14})$$

<sup>14</sup> In addition, we remark that the state  $|\varphi\rangle$  is not required to fulfill

the symmetry in (6).

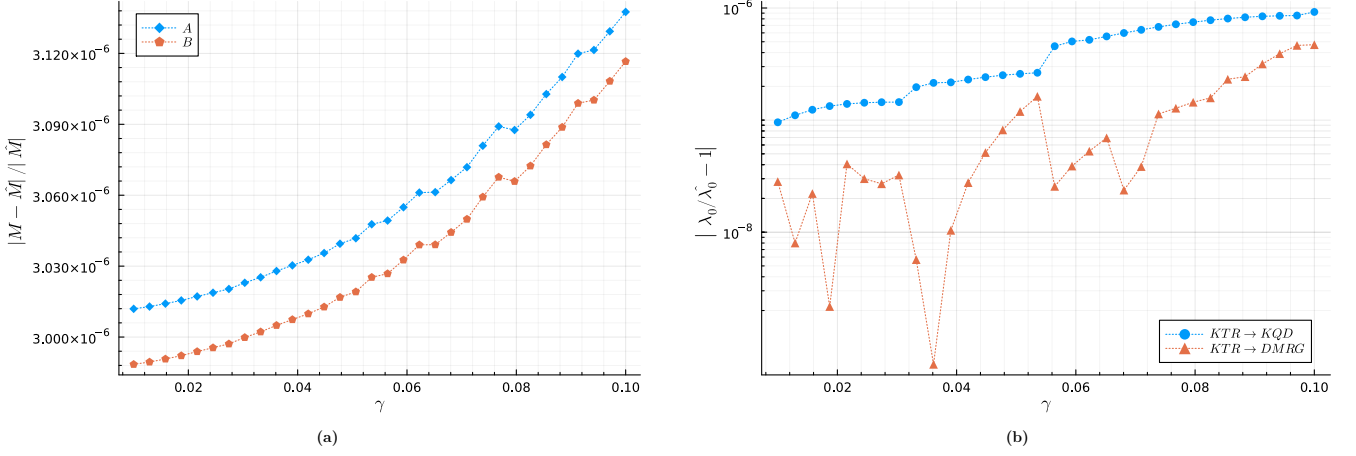


**FIG. 4:** Numerical demonstration (MPS) of [Theorem C.1](#) and [Theorem C.2](#) (implicit Hadamard test) for the TFIM on 64 qubits, reflecting the case of [Section V A](#) and [Figure 2](#). (a) Relative errors for the overlap matrices  $A$  and  $B$ , where reference quantities are computed using the RHSs of (C8) and (C14). (b) Relative error of the ground energy  $\lambda_0$  computed using the overlaps on the LHSs of (C8) and (C14). As references, we consider the canonical KQD ( $\bullet$ ) and DMRG ( $\blacktriangle$ ).

*Proof.* The pattern for this proof is very similar to that of [Theorem C.1](#). For a complex scalar  $z \in \mathbb{C}$  we denote by  $\Im z = (z - \bar{z})/(i2)$  its imaginary part. First, by the commutativity of  $\mathcal{H}$  and  $U^\dagger$  ( $U$  defined in [Theorem C.1](#)) we have that  $\text{Skew}(U\mathcal{H}) = \text{Skew}(U)\mathcal{H}$ , then

$$i \Im \langle \varphi | U\mathcal{H} | \varphi \rangle = \langle \varphi | \text{Skew}(U)\mathcal{H} | \varphi \rangle. \quad (\text{C15})$$

We aim to prove the following

$$\frac{1}{\xi^2} \langle v(t_a) | \mathcal{H} | v(t_b) \rangle - \left(1 - \frac{1}{\xi^2}\right) \langle v^\perp(t_a) | \mathcal{H} | v^\perp(t_b) \rangle = \langle \varphi | \text{Skew}(U)\mathcal{H} | \varphi \rangle, \quad (\text{C16})$$

which, as a result of [Lemma III.2](#) (with  $K = \mathcal{H}$ ), is equivalent to the claim in (C14).

Using the identities in [Lemma C.1](#) we obtain

$$PU\mathcal{H}P + P^\perp U\mathcal{H}P^\perp \stackrel{(\text{C5a})}{=} PUP^\perp\mathcal{H} + P^\perp UP\mathcal{H} \quad (\text{C17a})$$

$$\stackrel{(\text{C5b})}{=} \text{Skew}(U)P^\perp\mathcal{H} + \text{Skew}(U)P\mathcal{H} \quad (\text{C17b})$$

$$= \text{Skew}(U)\mathcal{H}, \quad (\text{C17c})$$

where the last equality follows from the complementarity of the projectors. We also observe the following identities similar<sup>15</sup> to those in (C5d), that is

$$P(U\mathcal{H})P = PT^2\sqrt{U}T^2\mathcal{H}\sqrt{U}P = P\sqrt{U}^\dagger(T\mathcal{H})\sqrt{U}P, \quad (\text{C18a})$$

$$P^\perp(U\mathcal{H})P^\perp = -P^\perp\sqrt{U}^\dagger(T\mathcal{H})\sqrt{U}P^\perp. \quad (\text{C18b})$$

Here we used the facts that  $PT = TP = P$  and  $P^\perp T = TP^\perp = -P^\perp$ , which follow from the definitions in (10).

Thus, by applying the preceding identities to (C16), we obtain

$$\frac{1}{\xi^2} (\xi \langle \varphi | P) U\mathcal{H} (\xi P | \varphi \rangle) + \left(1 - \frac{1}{\xi^2}\right) (\xi^\perp \langle \varphi | P^\perp) U\mathcal{H} (\xi^\perp P^\perp | \varphi \rangle) = \langle \varphi | \text{Skew}(U)\mathcal{H} | \varphi \rangle, \quad (\text{C19})$$

with  $\xi^\perp = \frac{\xi}{\sqrt{\xi^2 - 1}}$ . Hence, the latter together with (C15) confirms the claim.  $\square$

<sup>15</sup> Notably, these identities can be deduced from the proof of

[Lemma III.2](#), when  $K = \mathcal{H}$ .

In practice, the foregoing results determine the overlap matrices whose entries are defined by

$$A_{a,b} = i \Im \langle \varphi | U(t_b - t_a) \mathcal{H} | \varphi \rangle, \quad (\text{C20a})$$

$$B_{a,b} = \Re \langle \varphi | U(t_b - t_a) | \varphi \rangle, \quad (\text{C20b})$$

and whose computations are obtained using the LHS of respectively (C14) and (C8). In Figure 4 we provide a numerical demonstration of the implicit Hadamard test, using the same model considered in Section V A. The relative error for the ground energy is comparable with the previous results depicted in Figure 2 (specifically, see the series corresponding to  $s = 2$ ).

#### Appendix D: Localized projection circuit for initial states

We illustrate a strategy related to the construction of the initial states  $|v_0\rangle, |v_0^\perp\rangle$ , starting from an arbitrary state  $|\varphi\rangle$ , which we introduced in Section IV. In particular, we focus on the near-term implementability, so we consider states with localized entanglement. In essence, this formalizes the blocking pattern we used in the experiments in Section V A and Section V B. To achieve such a purpose, instead of considering the two complementary projectors  $P$  and  $P^\perp$  defined in (10), we construct a set of projectors  $\{P_i\}$  characterized by a convenient entanglement structure. We show that such a set can be partitioned into two subsets  $\mathcal{P} \cup \mathcal{P}^\perp$ , each distinguished by its elements  $P_i$  being orthogonal to either  $P$  or  $P^\perp$ .

We assume that the time reversal operator  $T$  is tensor separable into  $s$  operators<sup>16</sup>, that is  $T = \bigotimes_{i=1}^s T_b$ . Since  $T$  is Hermitian-involutory, the same property applies to the block operator  $T_b$ . In addition, we assume that the number of blocks  $s \ll n$ , where  $n$  is the number of qubits<sup>17</sup>. Consider the functions  $\alpha_i : \{1, \dots, s\} \rightarrow \{0, 1\}$  such that  $i_1 \neq i_2$  implies  $\sum_j |\alpha_{i_1}(j) - \alpha_{i_2}(j)| \neq 0$ . There are  $2^s$  distinct functions  $\alpha_i$ . Define the  $i$ th projector by

$$P_i := \bigotimes_{j=1}^s \frac{\mathbb{I} + (-1)^{\alpha_i(j)} T_b}{2}, \quad (\text{D1})$$

which is indeed an orthogonal projector since  $P_i^2 = \mathbb{I}$  and  $P_i^\dagger = P_i$ . The defining property of the functions  $\alpha_i$  implies that  $P_{i_1} P_{i_2} = 0$  whenever  $i_1 \neq i_2$ . Let  $p$  be the function on the set of functions  $\alpha_i$  with rule  $\alpha_i \mapsto (-1)^{\sum_j \alpha_i(j)}$ . Then we partition the set of projectors  $\{P_i\}$  into two subsets conditioned to value of the function<sup>18</sup>  $p$ , so

$$\mathcal{P} := \{P_i | p(\alpha_i) = 1\}, \quad \mathcal{P}^\perp := \{P_i | p(\alpha_i) = -1\}. \quad (\text{D2})$$

It can be shown that  $TP_i = p(\alpha_i)P_i$ , then

$$PP_i = P_i \frac{1 + p(\alpha_i)}{2}, \quad P^\perp P_i = P_i \frac{1 - p(\alpha_i)}{2}, \quad (\text{D3})$$

for all  $i$ , so we have either  $PP_i = P_i$  or  $P^\perp P_i = P_i$ . Hence, the sets  $\mathcal{P}$  and  $\mathcal{P}^\perp$  in (D2) can be defined equivalently as

$$\mathcal{P} = \{P_i | PP_i \neq 0\}, \quad \mathcal{P}^\perp = \{P_i | P^\perp P_i \neq 0\}. \quad (\text{D4})$$

For all  $i$ , and any (conformable) state  $|\varphi\rangle$ , we observe the following property

$$(T - p(\alpha_i)\mathbb{I}) P_i |\varphi\rangle = 0, \quad (\text{D5})$$

which corresponds to the stabilizer property in (6), with  $|v_0\rangle = \xi P_i |\varphi\rangle$  and  $c = p(\alpha_i)$  (see also Section IV), for some normalization coefficient  $\xi > 0$  (assuming  $P_i |\varphi\rangle \neq 0$ ).

<sup>16</sup> This condition is non-restrictive since for all models under consideration, the operator  $T$  consists of a tensor product of Pauli operators. In general, this is expected to hold for  $k$ -local Hamiltonians.

<sup>17</sup> Moreover, the number of blocks  $s$  is expected to depend at least

linearly on the number of qubits  $n$ . This prevents the overlap between the ground state and the initial state from decaying exponentially as  $n$  increases.

<sup>18</sup> We note that the function  $p$  can be interpreted as a parity function, since the sign of its image depends on the parity of  $\sum_j \alpha_i(j)$ .

**Lemma D.1.** Let  $P$  and  $P^\perp$  be the projectors defined in (10) and  $P_i$  those in (D1), then

$$\sum_{P_i \in \mathcal{P}} P_i = P, \quad \sum_{P_i \in \mathcal{P}^\perp} P_i = P^\perp, \quad (\text{D6})$$

so  $\sum_i P_i = \mathbb{I}$ .

*Proof.* For a single block, we note that  $(\mathbb{I} + T_b)/2 + (\mathbb{I} - T_b)/2 = \mathbb{I}$ , then consider the induction step where the projectors  $P_i$  act on  $s$  blocks. Assuming  $\sum_i P_i = \mathbb{I}$ , then for  $s + 1$  blocks we have that

$$\sum_i \left( \frac{\mathbb{I} + T_b}{2} \otimes P_i + \frac{\mathbb{I} - T_b}{2} \otimes P_i \right) = \mathbb{I} \otimes \mathbb{I}. \quad (\text{D7})$$

The proof is concluded by observing that  $\sum_i P_i = \mathbb{I} \implies P \sum_i P_i = P \xRightarrow{(\text{D4})} \sum_{P_i \in \mathcal{P}} P_i = P$ , and likewise for the second claim.  $\square$

This proves that the set  $\{P_i\}$  is a complete orthogonal set of projectors.

We now have the required structures for extending [Theorem C.1](#) as follows.

**Theorem D.1.** For any pair of time displacements  $t_a, t_b \in \mathbb{R}$ , we have that

$$\sum_{i=1}^{2^s} p(\alpha_i) \langle \varphi | P_i \left( \sqrt{U}^\dagger T \sqrt{U} \right) P_i | \varphi \rangle = \Re \langle \varphi | \sum_{i=1}^{2^s} (P_i U P_i) | \varphi \rangle, \quad (\text{D8})$$

with  $U = \exp(-i(t_b - t_a)\mathcal{H})$ . Also  $\sqrt{U} = \exp(-ih\mathcal{H})$  with  $h = (t_b - t_a)/2$ .

In particular, when  $\{P_i\} = \{P, P^\perp\}$ , then as a consequence of [Lemma C.1](#), the preceding theorem reduces to [Theorem C.1](#). An equivalent extension for [Theorem C.2](#) can be obtained using the same reasoning; we omit the result.

*Proof.* The proof follows the same reasoning as in [Theorem C.1](#). We outline the key steps. From (D3) we have that either  $P_i P \neq 0$  or  $P_i P^\perp \neq 0$ , assuming the former we have that  $P_i P = P_i$ . So from (C5c) and (C5d) it follows that

$$P_i U P_i = P_i \text{Herm}(U) P_i, \quad (\text{D9a})$$

$$P_i U P_i = p(\alpha_i) P_i \sqrt{U}^\dagger T \sqrt{U} P_i. \quad (\text{D9b})$$

When  $P_i P^\perp \neq 0$ , the result follows similarly, with attention to the negative sign in (C5d), which is realized by the expression  $p(\alpha_i)$ . We note that the mapping  $U \mapsto \sum_i P_i U P_i$  is a projection. Hence, the above identities and the relation in (C10), establish the claim in (D8).  $\square$

Using the following circuit identity recursively



$$(\text{D10})$$

In [Figure 5](#), we devise a circuit construction for the preparation of the initial states  $\{P_i |\varphi\rangle\}$ , based on the projectors in (D1). Such states can be used in conjunction with [Theorem D.1](#), to obtain the overlap matrices following the approach taken in (C20a). In [Figure 6](#) we provide a numerical demonstration of [Theorem D.1](#), using the same model considered in [Section V A](#).

*Remark 1.* In relation to the circuit in [Figure 5](#), when  $(\bigotimes_j U_j^\dagger)^{\otimes s} |\varphi\rangle$  is a computational basis state or a linear combination of fixed points of the permutation implemented by the first ladder of CNOTs, then the structure simplifies to a product of GHZ-like states<sup>19</sup> (without requiring additional qubits). The latter is the case for the benchmarks we considered in [Section V A](#) and [Section V B](#).

<sup>19</sup> We call these states GHZ-like since the circuit mirrors the struc-

ture of the *Greenberger-Horne-Zeilinger* state preparation.

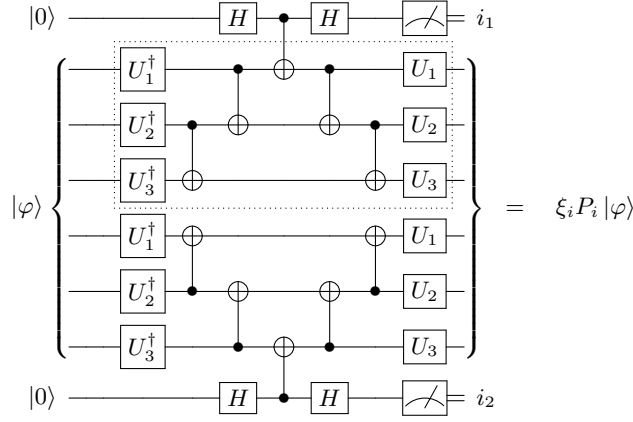


**FIG. 5:** General case for the projection  $P_i$  applied to the arbitrary state  $|\varphi\rangle$  (on  $n = 6$  qubits, with  $s = 2$  blocks) when the time reversal operator is of the form  $T = \bigotimes_{l=1}^n V_l$ , where  $V_l$  is a non-identity, single-qubit involutory unitary (e.g. Paulis). This pattern can be extended to any number of blocks, with each block requiring an additional qubit. The unitaries  $U_l$  satisfy the equation  $U_l \sigma^x U_l^\dagger = V_l$ , where  $V_l$  is the target unitary (with eigenvalues  $\{\pm 1\}$ ). The bits  $i_1, i_2$  define the index  $i = i_1 i_2$  determining the projection  $P_i$  in (D1). The coefficients  $\xi_i \in (0, +\infty]$  are defined such that  $\sum_i 1/\xi_i^2 = 1$ . We note that the state is defined when  $\xi_i$  is finite, that is, the probability  $1/\xi_i^2$  is non-zero.

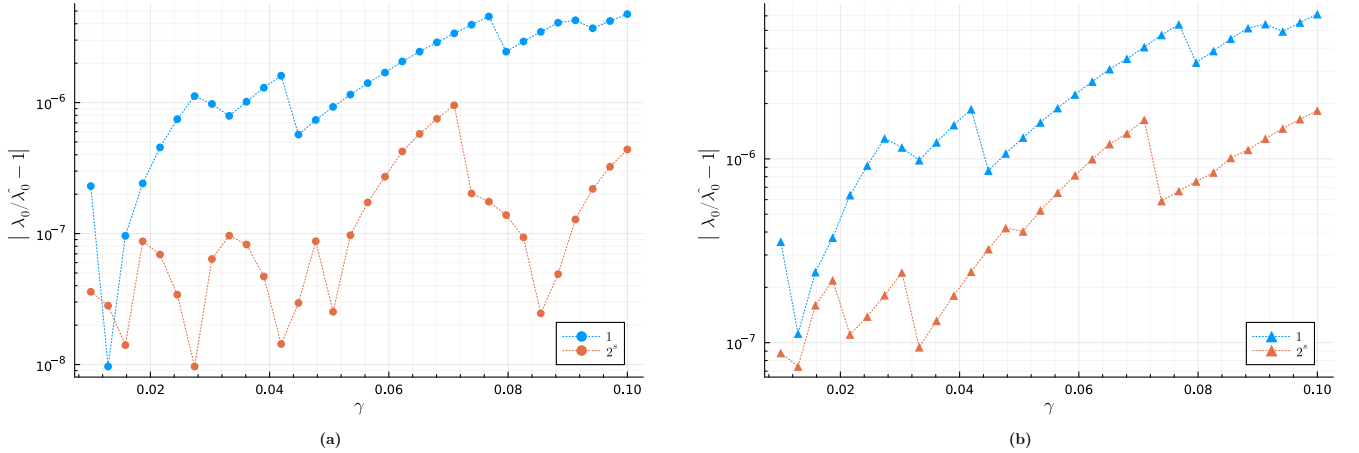


**FIG. 6:** Numerical demonstration (MPS) of [Theorem D.1](#) for the TFIM on 64 qubits, reflecting the case of [Section V A](#) and [Figure 2](#), with  $s = 4$  blocks. We plot the relative error of the ground energy  $\lambda_0$  computed using the initial states produced by the circuit in [Figure 5](#), with  $|\varphi\rangle = |+\rangle^{\otimes n}$ . As references, we consider the canonical KQD ( $\bullet$ , plot (a)) and DMRG ( $\blacktriangle$ , plot (b)). Here, the series are distinguished by the number of terms in (D8) (related to the projectors  $P_i$ ). The case  $2^s$  (i.e., all projectors) shows improved convergence.

## Appendix E: Additional Theoretical Considerations

In [Section II](#), we have shown that the KQD method requires the computation of the overlap matrices  $A$  and  $B$ , defining the generalized eigenvalue problem. However, when the conditions of [Section III](#) are fulfilled, we prove that we can obtain the entries of matrix  $B$  from the entries of  $A$  and vice versa, using quadrature [\[44\]](#) or derivative discretization [\[20\]](#) methods.

The result that follows can be framed as a further consequence of the implication  $\{\mathcal{H}, T\} = 0 \implies \frac{1}{2}[\imath\mathcal{H}, T] = \imath\mathcal{H}T$ . Before, we introduce the *Kubo formula* [\[45, 46\]](#). For square matrices  $A, B$  of the same size, we have that

$$[A, e^{-\imath t B}] = -\imath e^{-\imath t B} \int_0^t e^{\imath \tau B} [A, B] e^{-\imath \tau B} d\tau, \quad (\text{E1})$$

for all  $t \in \mathbb{R}$ .

**Lemma E.1.** Assuming the conditions of [Lemma III.1](#) and [Lemma III.2](#) (with  $K = \mathcal{H}$ ), we have that

$$2c \int_0^h \langle v(\tau) | (i\mathcal{H}T) | v(\tau) \rangle d\tau + 1 = c \langle v(h) | T | v(h) \rangle, \quad (\text{E2a})$$

$$\frac{ic}{2} \frac{d}{dh} \langle v(h) | T | v(h) \rangle = ic \langle v(h) | (i\mathcal{H}T) | v(h) \rangle. \quad (\text{E2b})$$

*Proof.* Considering the Hamiltonian  $\mathcal{H}$  and a corresponding time reversal operator  $T$ , we rewrite the Kubo formula in [\(E1\)](#) as follows

$$\int_0^h e^{i\tau\mathcal{H}} [i\mathcal{H}, T] e^{-i\tau\mathcal{H}} d\tau = e^{ih\mathcal{H}} [T, e^{-ih\mathcal{H}}], \quad (\text{E3})$$

where the RHS sandwiched between  $\langle v_0 | \cdots | v_0 \rangle$  expands as

$$\langle v_0 | e^{ih\mathcal{H}} [T, e^{-ih\mathcal{H}}] | v_0 \rangle = \langle v_0 | e^{ih\mathcal{H}} T e^{-ih\mathcal{H}} | v_0 \rangle - \langle v_0 | T | v_0 \rangle \quad (\text{E4a})$$

$$\stackrel{(1),(6)}{=} \langle v(h) | T | v(h) \rangle - c. \quad (\text{E4b})$$

Then, noting that  $c^2 = 1$  (as explained in [Section III](#),  $c \in \{\pm 1\}$ )

$$c \int_0^h \langle v(\tau) | [i\mathcal{H}, T] | v(\tau) \rangle d\tau = c \langle v(h) | T | v(h) \rangle - 1. \quad (\text{E5})$$

Hence, the claim in [\(E2a\)](#) follows from the relation  $\frac{1}{2}[i\mathcal{H}, T] = i\mathcal{H}T$ . Using the same relation, we deduce the second claim, so

$$\frac{1}{2} \frac{d}{dh} \langle v(h) | T | v(h) \rangle \stackrel{(1)}{=} \frac{1}{2} \langle v(h) | (i\mathcal{H}T) | v(h) \rangle - \frac{1}{2} \langle v(h) | (iT\mathcal{H}) | v(h) \rangle \quad (\text{E6a})$$

$$= \frac{1}{2} \langle v(h) | [i\mathcal{H}, T] | v(h) \rangle \quad (\text{E6b})$$

$$= \langle v(h) | (i\mathcal{H}T) | v(h) \rangle. \quad (\text{E6c})$$

□

In the preceding claim, we note that the arguments of the integral and derivative, and the expressions on the RHSs, correspond interchangeably to the RHSs of main results in [\(8\)](#) and [\(7\)](#) (up to a constant factor).

Suppose  $H = \sum_{i=1}^L h_i \sigma_i$  for  $\sigma_i \in \{\mathbb{I}, \sigma^x, \sigma^y, \sigma^z\}^{\otimes n}$  and  $h_i \in \mathbb{C}$ . Computing the matrices  $A$  and  $B$  directly via [\(9\)](#) and [\(7\)](#) requires  $m$  and  $Lm$  expectation values, respectively. A natural strategy, therefore, is to construct  $B$  directly using [\(7\)](#), and then numerically estimate  $A$  via the relation [\(E2b\)](#), with the inherent overhead of additional time samples required for accurate derivative estimation. [Figure 7](#) presents a numerical demonstration of this strategy, alongside the complementary approach where  $A$  is computed directly using [\(9\)](#), and  $B$  is estimated numerically via [\(E2a\)](#). For derivative estimation, we employ the regularized state-space approach proposed in [\[20\]](#). For integral estimation, we utilize the composite Simpson's rule [\[47\]](#).



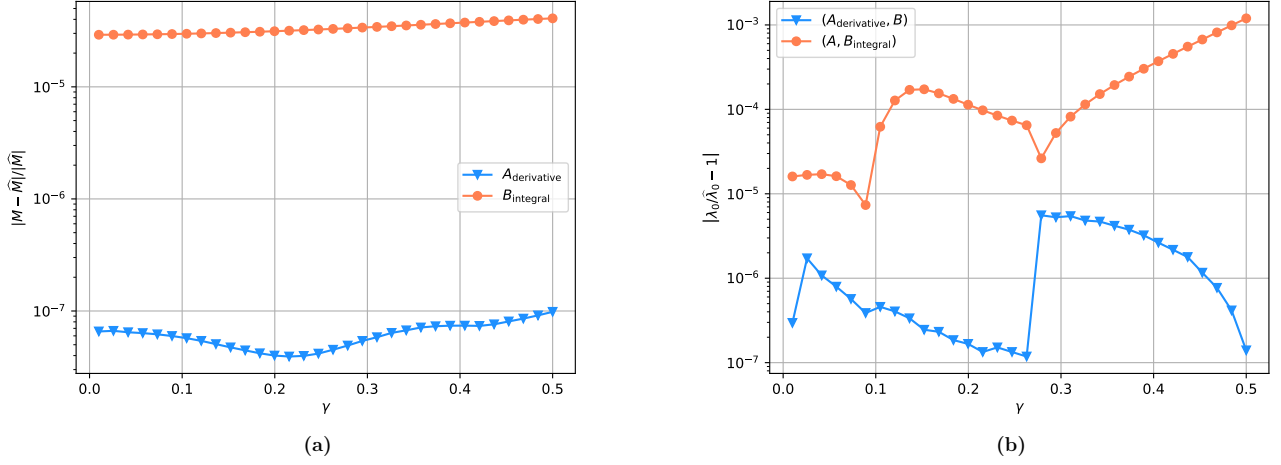


**FIG. 7:** Numerical demonstration (MPS) of Lemma E.1 for the TFIM on 48 qubits, with Krylov dimension  $m = 10$ . The matrices  $A_{\text{derivative}}$  and  $B_{\text{integral}}$  are estimated numerically via the relations (E2b) and (E2a) respectively, using  $20m$  sampling points. (a) Relative error for the overlap matrices  $A_{\text{derivative}}$  and  $B_{\text{integral}}$ , with references to the quantities  $A$  and  $B$  computed via (9) and (7) respectively. (b) Relative error of the ground energy  $\lambda_0$  of the pencils  $(A_{\text{derivative}}, B)$  and  $(A, B_{\text{integral}})$ , with reference to the ground energy of  $(A, B)$ .

- 
- [1] R. M. Parrish and P. L. McMahon, [Quantum filter diagonalization: Quantum eigendecomposition without full quantum phase estimation](#) (2019), [arXiv:1909.08925 \[quant-ph\]](#).
  - [2] N. H. Stair, R. Huang, and F. A. Evangelista, A multireference quantum krylov algorithm for strongly correlated electrons, *Journal of Chemical Theory and Computation*, **Journal of Chemical Theory and Computation** **16**, 2236 (2020).
  - [3] J. Cohn, M. Motta, and R. M. Parrish, Quantum filter diagonalization with compressed double-factorized hamiltonians, *PRX Quantum* **2**, 040352 (2021).
  - [4] K. Klymko, C. Mejuto-Zaera, S. J. Cotton, F. Wudarski, M. Urbanek, D. Hait, M. Head-Gordon, K. B. Whaley, J. Moussa, N. Wiebe, W. A. de Jong, and N. M. Tubman, Real-time evolution for ultracompact hamiltonian eigenstates on quantum hardware, *PRX Quantum* **3**, 020323 (2022).
  - [5] C. L. Cortes and S. K. Gray, Quantum krylov subspace algorithms for ground- and excited-state energy estimation, *Phys. Rev. A* **105**, 022417 (2022).
  - [6] K. Seki and S. Yunoki, Quantum power method by a superposition of time-evolved states, *PRX Quantum* **2**, 010333 (2021).
  - [7] Y. Shen, K. Klymko, J. Sud, D. B. Williams-Young, W. A. d. Jong, and N. M. Tubman, Real-time krylov theory for quantum computing algorithms, *Quantum* **7**, 1066 (2023).
  - [8] W. Kirby, M. Motta, and A. Mezzacapo, Exact and efficient lanczos method on a quantum computer, *Quantum* **7**, 1018 (2023).
  - [9] M. Motta, C. Sun, A. T. K. Tan, M. J. O'Rourke, E. Ye, A. J. Minnich, F. G. S. L. Brandão, and G. K.-L. Chan, Determining eigenstates and thermal states on a quantum computer using quantum imaginary time evolution, *Nature Physics* **16**, 205 (2020).
  - [10] M. Motta, W. Kirby, I. Liepuoniute, K. J. Sung, J. Cohn, A. Mezzacapo, K. Klymko, N. Nguyen, N. Yoshioka, and J. E. Rice, Subspace methods for electronic structure simulations on quantum computers, *Electronic Structure* **6**, 10.1088/2516-1075/ad3592 (2024).
  - [11] N. Yoshioka, M. Amico, W. Kirby, P. Jurcevic, A. Dutt, B. Fuller, S. Garion, H. Haas, I. Hamamura, A. Ivrii, R. Majumdar, Z. Mineev, M. Motta, B. Pokharel, P. Rivero, K. Sharma, C. J. Wood, A. Javadi-Abhari, and A. Mezzacapo, Krylov diagonalization of large many-body hamiltonians on a quantum processor, *Nature Communications* **16**, 5014 (2025).
  - [12] J. Yu, J. R. Moreno, J. T. Iosue, L. Bertels, D. Claudino, B. Fuller, P. Groszkowski, T. S. Humble, P. Jurcevic, W. Kirby, T. A. Maier, M. Motta, B. Pokharel, A. Seif, A. Shehata, K. J. Sung, M. C. Tran, V. Tripathi, A. Mezzacapo, and K. Sharma, [Quantum-centric algorithm for sample-based krylov diagonalization](#) (2025), [arXiv:2501.09702 \[quant-ph\]](#).
  - [13] J. Robledo-Moreno, M. Motta, H. Haas, A. Javadi-Abhari, P. Jurcevic, W. Kirby, S. Martiel, K. Sharma, S. Sharma, T. Shirakawa, I. Shtedlikov, R.-Y. Sun, K. J. Sung, M. Takita, M. C. Tran, S. Yunoki, and A. Mezzacapo, Chemistry beyond the scale of exact diagonalization on a quantum-centric supercomputer, *Science Advances* **11**, eadu9991 (2025), <https://www.science.org/doi/pdf/10.1126/sciadv.adu9991>.
  - [14] A. Duriez, P. C. Carvalho, M. A. Barroca, F. Zipoli, B. Jaderberg, R. N. B. Ferreira, K. Sharma, A. Mezzacapo, B. Wunsch, and M. Steiner, [Computing band gaps of periodic materials via sample-based quantum diagonalization](#) (2025), [arXiv:2503.10901 \[quant-ph\]](#).
  - [15] O. Oumarou, P. J. Ollitrault, C. L. Cortes, M. Scheurer, R. M. Parrish, and C. Gogolin, [Molecular properties from quantum krylov subspace diagonalization](#) (2025), [arXiv:2501.05286 \[quant-ph\]](#).
  - [16] E. N. Epperly, L. Lin, and Y. Nakatsukasa, A theory of quantum subspace diagonalization, *SIAM Journal on Matrix Analysis and Applications* **43**, 1263 (2022), <https://doi.org/10.1137/21M145954X>.
  - [17] W. Kirby, Analysis of quantum Krylov algorithms with errors, *Quantum* **8**, 1457 (2024).
  - [18] J. Preskill, Quantum computing in the nisq era and beyond, *Quantum* **2**, 79 (2018).
  - [19] B. F. Schiffer, D. S. Wild, N. Maskara, M. D. Lukin, and J. I. Cirac, [Hardware-efficient quantum phase estimation via local control](#) (2025), [arXiv:2506.18765 \[quant-ph\]](#).
  - [20] A. Byrne, W. Kirby, K. M. Soodhalter, and S. Zhuk, [A quantum-centric super-krylov diagonalization method](#) (2024), [arXiv:2412.17289 \[quant-ph\]](#).
  - [21] Y. Yang, A. Christianen, M. C. Bañuls, D. S. Wild, and J. I. Cirac, Phase-sensitive quantum measurement without controlled operations, *Phys. Rev. Lett.* **132**, 220601 (2024).
  - [22] A. Chowdhury, E. van den Berg, and P. Wocjan, [Controlization schemes based on orthogonal arrays](#) (2025), [arXiv:2407.09382 \[quant-ph\]](#).
  - [23] A. N. Krylov, On the numerical solution of the equation by which in technical questions frequencies of small oscillations of material systems are determined, *Izvestiya Akademii Nauk SSSR, Otdelenie Fiziko-Matematicheskikh Nauk* **7**, 491 (1931).
  - [24] G. H. Golub and C. F. Van Loan, *Matrix Computations - 4th Edition* (Johns Hopkins University Press, Philadelphia, PA, 2013) <https://epubs.siam.org/doi/pdf/10.1137/1.9781421407944>.
  - [25] R. A. Horn and C. R. Johnson, *Matrix Analysis*, 2nd ed. (Cambridge University Press, 2012).
  - [26] E. Knill, G. Ortiz, and R. D. Somma, Optimal quantum measurements of expectation values of observables, *Phys. Rev. A* **75**, 012328 (2007).
  - [27] M. A. Nielsen and I. L. Chuang, *Quantum Computation and Quantum Information: 10th Anniversary Edition* (Cambridge University Press, 2010).
  - [28] D. Tao and M. Yasuda, A spectral characterization of generalized real symmetric centrosymmetric and generalized real symmetric skew-centrosymmetric matrices, *SIAM Journal on Matrix Analysis and Applications* **23**, 885 (2002), <https://doi.org/10.1137/S0895479801386730>.

- [29] R. Orús, A practical introduction to tensor networks: Matrix product states and projected entangled pair states, *Annals of Physics* **349**, 117–158 (2014).
- [30] C. Hubig, I. P. McCulloch, and U. Schollwöck, Generic construction of efficient matrix product operators, *Phys. Rev. B* **95**, 035129 (2017).
- [31] D. Malz, G. Styliaris, Z.-Y. Wei, and J. I. Cirac, Preparation of matrix product states with log-depth quantum circuits, *Phys. Rev. Lett.* **132**, 040404 (2024).
- [32] N. Robertson, A. Akhriev, J. Vala, and S. Zhuk, Approximate quantum compiling for quantum simulation: A tensor network based approach, *ACM Transactions on Quantum Computing* **10.1145/3731251** (2025).
- [33] M. Fishman, S. R. White, and E. M. Stoudenmire, The ITensor Software Library for Tensor Network Calculations, *SciPost Phys. Codebases*, **4** (2022).
- [34] N. Hatano and M. Suzuki, Finding exponential product formulas of higher orders, in *Quantum Annealing and Other Optimization Methods* (Springer Berlin Heidelberg, 2005) p. 37–68.
- [35] S. Paeckel, T. Köhler, A. Swoboda, S. R. Manmana, U. Schollwöck, and C. Hubig, Time-evolution methods for matrix-product states, *Annals of Physics* **411**, 167998 (2019).
- [36] U. Schollwöck, The density-matrix renormalization group in the age of matrix product states, *Annals of Physics* **326**, 96 (2011), january 2011 Special Issue.
- [37] E. Bäumer, V. Tripathi, D. S. Wang, P. Rall, E. H. Chen, S. Majumder, A. Seif, and Z. K. Mineev, Efficient long-range entanglement using dynamic circuits, *PRX Quantum* **5**, 030339 (2024).
- [38] J. Cobos, J. Fraxanet, C. Benito, F. di Marcantonio, P. Rivero, K. Kapás, M. A. Werner, Örs Legeza, A. Bermudez, and E. Rico, *Real-time dynamics in a (2+1)-d gauge theory: The stringy nature on a superconducting quantum simulator* (2025), [arXiv:2507.08088 \[quant-ph\]](https://arxiv.org/abs/2507.08088).
- [39] E. Fradkin and S. H. Shenker, Phase diagrams of lattice gauge theories with higgs fields, *Phys. Rev. D* **19**, 3682 (1979).
- [40] W.-T. Xu, T. Rakovszky, M. Knap, and F. Pollmann, Entanglement properties of gauge theories from higher-form symmetries, *Phys. Rev. X* **15**, 011001 (2025).
- [41] S. Bravyi, J. M. Gambetta, A. Mezzacapo, and K. Temme, *Tapering off qubits to simulate fermionic hamiltonians* (2017), [arXiv:1701.08213 \[quant-ph\]](https://arxiv.org/abs/1701.08213).
- [42] D. Knuth, *The Art of Computer Programming: Combinatorial Algorithms, Volume 4B*, The Art of Computer Programming No. pt. 2 (Pearson Education Canada, 2021).
- [43] A. Smith, B. Jobst, A. G. Green, and F. Pollmann, Crossing a topological phase transition with a quantum computer, *Phys. Rev. Res.* **4**, L022020 (2022).
- [44] G. H. Golub and J. H. Welsch, Calculation of gauss quadrature rules, in *Milestones in Matrix Computation* (1967).
- [45] R. Kubo, Statistical-mechanical theory of irreversible processes. i. general theory and simple applications to magnetic and conduction problems, *Journal of the Physical Society of Japan* **12**, 570 (1957), <https://doi.org/10.1143/JPSJ.12.570>.
- [46] M. Suzuki, Decomposition formulas of exponential operators and lie exponentials with some applications to quantum mechanics and statistical physics, *Journal of Mathematical Physics* **26**, 601 (1985), [https://pubs.aip.org/aip/jmp/article-pdf/26/4/601/19120226/601\\_1\\_online.pdf](https://pubs.aip.org/aip/jmp/article-pdf/26/4/601/19120226/601_1_online.pdf).
- [47] P. J. Davis and P. Rabinowitz, *Methods of numerical integration* (Courier Corporation, 2007).